High-order harmonic generation in a crystalline solid

L. Plaja*
Departament de Física, Universitat Autònoma de Barcelona, 08193 Bellaterra, Spain

L. Roso-Franco†
Departamento de Física Aplicada, Universidad de Salamanca, 37008 Salamanca, Spain

(Received 8 August 1991)

The interaction between a laser field and a crystalline solid is considered. The electron wave function in the crystal is obtained from an appropriately chosen pseudopotential. The dipole approximation is introduced, and only vertical transitions are taken into account. We present a nonperturbative method based on the numerical computation of solutions of the Schrödinger equation, to obtain the generation of harmonics of the incident laser. Particular numerical results are presented for the case of pure silicon. The mechanisms to enhance harmonic generation without excessive excitation of electrons to the conduction band are analyzed.

I. INTRODUCTION

High-order harmonic generation is a promising technique to obtain new sources of coherent radiation in the ultraviolet and soft-x-ray regions. A lot of theoretical work[1,2] and some experiments[3,4] have been reported that study the high-order harmonic generation accompanying multiphoton ionization of atoms in intense laser fields. These studies show that, to reach high-order harmonics, an intense pump laser is necessary which implies short pulses and total destruction (ionization) of the interacting material.

In this paper we study the response of a semiconductor to a very short (femtosecond) and very intense (over 10^{10} W/cm^2) laser pulse. Our objective is to analyze the possibility of harmonic generation without the necessity of a total destruction of the material. This should open the possibility of obtaining longer interaction regions and better repetition rates. To do this we propose using a crystalline solid structure instead of a low pressure gas. From atomic studies, it is clear that a new domain of nonlinear optics is encountered in the regime of very high pump intensities, possibly associated with the breakdown of conventional radiative perturbation theory. Therefore, a nonperturbative approach is presented to study the interaction of an intense laser pulse with a crystalline solid.

To illustrate these ideas, we will restrict our discussion to the case of pure silicon, and to harmonics up to the ninth. However, the presented formalism is quite general, provided that a pseudopotential can be introduced to account for the electronic states. Due to the relatively small gap of silicon, all harmonics considered in this paper are close to the visible region. A proper scaling of the conclusions to other crystalline structure is obviously possible.

II. ELECTRON-STATE MODEL

It is well known that a proper description of the electron properties in the crystal can be obtained using a single-electron model with a convenient choice of the crystal potential $V_c(\mathbf{r})$. Therefore, the crystal Hamiltonian is of the form

$$H_c(\mathbf{r}) = -\tfrac{1}{2}\nabla^2 + V_c(\mathbf{r}) , \tag{1}$$

where atomic units have been used ($\hbar = m = e = 1$).

Due to the periodicity of the crystal Hamiltonian, one may choose to work in a basis of Bloch functions, $\psi_{\mathbf{k},n}(\mathbf{r})$, satisfying

$$\psi_{\mathbf{k},n}(\mathbf{r}+\mathbf{l}) = e^{i\mathbf{k}\cdot\mathbf{l}}\psi_{\mathbf{k},n}(\mathbf{r}) , \tag{2}$$

$\mathbf{k}$ being a vector of the first Brillouin zone, $\mathbf{L}$ a lattice vector, and n a label for the energy bands. These Bloch states are eigenfunctions of the crystal Hamiltonian $H_c(\mathbf{r})$,

$$H_c(\mathbf{r})\psi_{\mathbf{k},n}(\mathbf{r}) = E_n^{\mathbf{k}}\psi_{\mathbf{k},n}(\mathbf{r}) , \tag{3}$$

and the $E_n^{\mathbf{k}}$, for the same $\mathbf{k}$ and different n, correspond to different electron energy bands.

III. SILICON BAND STRUCTURE

In this paper we want to discuss the processes that lead to harmonic generation by the interaction of a laser beam with a solid crystalline structure. A general analysis of the relation between energy bands and harmonic generation would be desirable, but this is too long and implies many different possibilities. Therefore we have restricted the scope of this paper to a particular crystalline structure. We have chosen to study silicon (see Fig. 1).

At present, the state-of-the-art silicon technology is advanced enough to achieve large and high-quality single crystals, and thus to match our specifications. In addition, optical properties, such as absorption coefficients, reflectivities, dielectric constants, and nonlinear susceptibilities for different frequencies, have been extensively studied and compared with the pseudopotential calculations.[5] Under a practical point of view, silicon offers an almost constant direct-gap interval, which helps in the

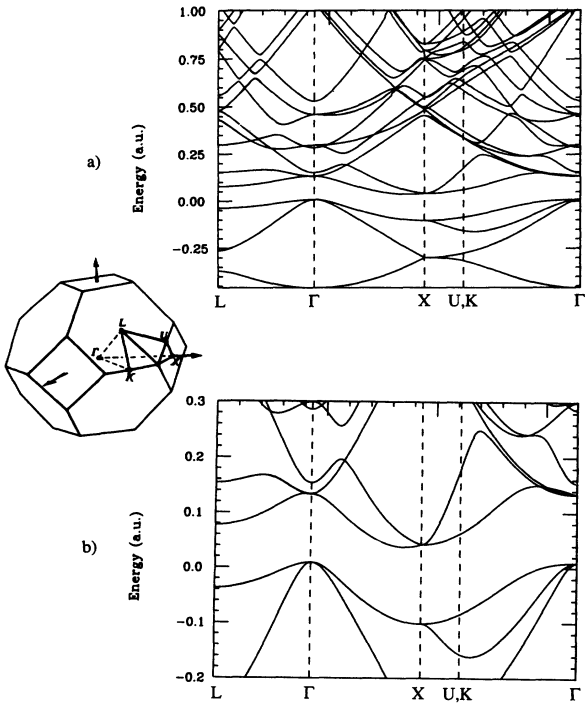

FIG. 1. Silicon electronic band structure considered. (a) The band structure obtained from the pseudopotential given in the text. (b) A detail of this band structure around the gap. The inset represents the first Brillouin zone, indicating the symmetry lines represented.

determination of the resonance-photon energies for transitions from the uppermost valence band to the lowest conduction bands. On the computational side, the choice of a semiconductor whose base is formed by two identical atoms implies the use of only symmetrical pseudopotential terms, and thus the use of real arithmetics, which means a reduction in computing time and memory storage requirements.

Before the study of the interaction with the laser field, we prefer to introduce some considerations related to the energy bands that will be relevant later on. The energy bands are obtained from (1) with a convenient choice of the pseudopotential, $V_{\rm ps}$.[6-8] The pseudopotential terms for the diamond structure are given by

$$V_{\rm ps}(\mathbf{g})=S_{\rm fcc}(\mathbf{g})V^s_{|\mathbf{g}|^2}\cos(\mathbf{g}\cdot\tau) , \tag{4}$$

where $S_{\rm fcc}(\mathbf{g})$ denotes the structure factor for a face-centered-cubic lattice, $\tau=a_0/8(1,1,1)$, a_0 being the length of the conventional cell. In the case of silicon, $a_0=5.43$ Å$=10.26$ a.u. The coefficients $V^s_{|\mathbf{g}|^2}$ are the symmetric form factors[9]

$$V^s_3=-0.21\ \text{Ry}=-0.105\ \text{a.u.}, \tag{5a}$$

$$V^s_8=+0.04\ \text{Ry}=+0.020\ \text{a.u.}, \tag{5b}$$

$$V^s_{11}=+0.08\ \text{Ry}=+0.040\ \text{a.u.}, \tag{5c}$$

where $|\mathbf{g}|^2$ has been computed in units of $|2\pi/a_0|^2$.

The eigenvalues and eigenstates of (3) with the crystal potential have been obtained by a tridiagonal reduction followed by the diagonalization of the tridiagonal matrix.[10,11] The number of calculated energy bands ranges from 60 to 100, depending on the point of the reciprocal space we are considering and on the photon energy we are going to use for the temporal evolution. Before scanning through the reciprocal space, an initial value of the number of bands to be computed is obtained from the Γ point, $\mathbf{k}=(0,0,0)$. It is the highest symmetry point, and thus will show the highest degeneration. We use it to evaluate the lowest limit of the considered energies: we have chosen the number of bands so that this limit is over 30 photon energy units. Due to this truncation we expect higher-energy bands not to be properly defined, so we restrict ourselves to the study of absorption of less than 20 photons.

The last consideration related with the cutoff of the energy bands is that for any point $\mathbf{k}$ one needs to take into account whole sets of degenerate bands. Otherwise symmetry will be broken and the matrix elements between the states will be severely disturbed. Thus, the final number of bands must be flexible and chosen for every point in the reciprocal space.

IV. LASER-ELECTRON INTERACTION

The dynamics of each electron is given by a Hamiltonian of the form

$$H(\mathbf{r},t)=H_c(\mathbf{r})+H_{\rm int}(t) , \tag{6}$$

where H_c is the crystal Hamiltonian, introduced in (1), and $H_{\rm int}$ is the laser-electron interaction Hamiltonian. In the dipole approximation and in the Coulomb gauge, $H_{\rm int}$ is given by

$$H_{\rm int}(t)=\frac{1}{2c^2}A^2(t)-i\frac{1}{c}A(t)\frac{\partial}{\partial z} , \tag{7}$$

where a linearly polarized laser, along the z axis, has been considered. $A(t)$ is the vector potential, which is integrated from the electric field,

$$A(t)=-\frac{1}{c}\int_0^t E(\tau)d\tau , \tag{8}$$

where

$$E(\tau)=E_0(\tau)\sin(\omega_L t). \tag{9}$$

For the computations presented in this paper, the electric-field envelope $E_0(\tau)$ has been taken in the form of a half-period square sine function,

$$E_0(\tau)=E\sin^2\left[\pi\frac{\tau}{\tau_p}\right] , \tag{10}$$

τ_p being the pulse duration. Here we will always consider pulses with a duration equal to 30 optical cycles, i.e., with $\tau_p=60\pi/\omega_L$.

Our objective is to obtain exact, nonperturbative solutions of the time-dependent Schrödinger equation,

$$i\frac{\partial\phi(\mathbf{r},t)}{\partial t}=[H_c(\mathbf{r})+H_{\rm int}(t)]\phi(\mathbf{r},t) . \tag{11}$$

Because the dipole interaction has been introduced, the laser field $E(\tau)$ is considered to be independent of the position of the electron. Therefore, we can take advantage of the spatial periodicity, since it is the only space dependence appearing in the Hamiltonian.

If we consider the basis of Bloch functions, $\psi_{\mathbf{k},n}(\mathbf{r})$, eigenfunctions of H_c, it is straightforward to see that H_{int} couples only Bloch states $\psi_{\mathbf{k},n}(\mathbf{r})$ and $\psi_{\mathbf{k}',n'}(\mathbf{r})$ with $\mathbf{k}=\mathbf{k}'$ ($\mathbf{k}',\mathbf{k}'$ belonging to the first Brillouin zone). Therefore, the dipole approximation is equivalent to considering only vertical optical transitions, in which the change of pseudomomentum, $\mathbf{k}'-\mathbf{k}$, induced by the absorption of laser photons is neglected.

In conclusion, $\mathbf{k}$ is a good label for the solutions of the time-dependent Schrödinger equation (11) in the dipole approximation. This means that each point of the reciprocal space evolves as a multiple-level system independently from its neighbor points.

A general solution can be written in the form

$$\phi_{\mathbf{k}}(\mathbf{r},t)=\sum_n c_n^{\mathbf{k}}(t)\psi_{\mathbf{k},n}(\mathbf{r}) \ . \tag{12}$$

V. HARMONIC GENERATION

The harmonic generation, i.e., the rate for generating photons at a frequency equal to a harmonic of the incident laser, is calculated from the quantum-mechanical dipole moment of the solid. For a given value of $\mathbf{k}$, the expected value in the $\mathbf{p}\cdot\mathbf{A}$ gauge is

$$p_{\mathbf{k}}(t)=\left\langle \phi_{\mathbf{k}}(\mathbf{r},t)\left|(-i)\frac{\partial}{\partial z}\right|\phi_{\mathbf{k}}(\mathbf{r},t)\right\rangle + \left\langle \phi_{\mathbf{k}}(\mathbf{r},t)\left|\frac{1}{c}A(t)\right|\phi_{\mathbf{k}}(\mathbf{r},t)\right\rangle \ , \tag{13}$$

that is,

$$p_{\mathbf{k}}(t)=\left\langle \phi_{\mathbf{k}}(\mathbf{r},t)\left|(-i)\frac{\partial}{\partial z}\right|\phi_{\mathbf{k}}(\mathbf{r},t)\right\rangle+\frac{1}{c}A(t) \ , \tag{14}$$

and, integrating over the first Brillouin zone,

$$p(t)=\sum_{\mathbf{k}}\left[\left\langle \phi_{\mathbf{k}}(\mathbf{r},t)\left|(-i)\frac{\partial}{\partial z}\right|\phi_{\mathbf{k}}(\mathbf{r},t)\right\rangle+\frac{1}{c}A(t)\right] \ . \tag{15}$$

The rate for generating photons of frequency ω is given by the Fourier transform of $p(t)$, which we will denote $p(\omega)$. Therefore the photon spectra that we present in this paper is, as usual, $|p(\omega)|^2$.[12] All our present physical discussion is related to these harmonic spectra; propagation effects will be not considered.

To calculate the expectation values $p_{\mathbf{k}}(t)$, it is more convenient to consider a plane-wave basis instead of the Bloch expansion,

$$\phi_{\mathbf{k}}(\mathbf{r},t)=\sum_{\mathbf{g}}\beta_{\mathbf{g}}^{\mathbf{k}}(t)e^{i(\mathbf{k}+\mathbf{g})\cdot\mathbf{r}} \ , \tag{16}$$

$\mathbf{g}$ being the vectors of the reciprocal lattice, because in this basis $p_{\mathbf{k}}(t)$ is simply given by

$$p_{\mathbf{k}}(t)=\sum_{\mathbf{g}}|\beta_{\mathbf{g}}^{\mathbf{k}}(t)|^2(k_z+g_z)+\frac{1}{c}A(t) \ . \tag{17}$$

The connection between the Bloch basis and the plane wave expansion is given by a collection of coefficients, $\alpha_{\mathbf{g}}^{\mathbf{k},n}$, such that

$$\psi_{\mathbf{k},n}(\mathbf{r})=\sum_{\mathbf{g}}\alpha_{\mathbf{g}}^{\mathbf{k},n}e^{i(\mathbf{k}+\mathbf{g})\cdot\mathbf{r}} \ . \tag{18}$$

These coefficients were calculated when we diagonalized the crystal Hamiltonian H_c.

VI. ELECTRON POPULATIONS

Up to now we have considered the dynamics of a single electron. However, we have to describe the overall interaction of the electrons with the laser field. To do this we have defined what is the interesting range of parameters and we introduce adequated approximations.

First of all we must remember that a pseudopotential has been introduced to describe the energy bands. For this model to be valid we need to have most of the electron population remaining in their lowest-energy states. In other words, if the laser excites an important number of electrons, the pseudopotential must change. However, this is not a problem for us because we want to propose harmonic-generation schemes in a "nondestructive way," i.e., exciting a reduced number of electrons but giving rise to relative high-order harmonics. Therefore the calculations presented in this paper correspond to situations where just a small number of electrons are promoted from the valence to the conduction band.

Apparently, as one increases the laser intensity, higher harmonics could be generated. However, this is not completely true, because the increase in the laser intensity pumps more and more electrons from the valence to the conduction band. When the number of electrons pumped to the valence band is a significant fraction of the electron density, our description of the crystal is no longer valid because the pseudopotential has to include the different effect of the excited electrons.

It is important to indicate the range of times we will consider. As pointed out before, only pulses 30 cycles long will be studied. With laser frequencies in the region between 0.05 and 0.2 a.u., this implies pulse durations of 942 to 3770 a.u., i.e., from 22 to 91 fs. This is a long time for electron dynamics but very short for phonon excitation. Therefore it seems reasonable to neglect collisional relaxation of excited electrons during the interaction time.

After the excitation, however, the energy absorbed might be non-negligible, depending on the amount of electrons excited to the conduction bands. In the worst case, where the laser is resonant with the direct gap, the remaining valence-band population after the pulse is about 95% for the two upper bands and almost 100% at the two lower bands. In such a nonequilibrium condition, nonradiative Auger processes become dominant. Neglecting heat conduction, a simple calculation indicates that the temperature rise is enough to exceed the melting point of Si (1690 K). Therefore, the interaction region will be melted. However, the released energy is

not enough to melt the whole sample, and the surrounding crystal will act as a heat absorber and as a recrystallization seed. As a matter of fact, the case is analogous to the laser-annealing technique. Typically, if the cooling time is longer than the time required for epitaxial regrowth, we can expect to recover the sample completely.[13] After recrystallization the solid is ready to start a new lasing cycle. Observe that the pulses considered here are extremely short. With longer pulses other mechanisms rather than coherent electron-photon interaction dominate the energy absorption and lead to damage of the crystal.

Initially we have four valence bands, with two electrons each. Obviously transitions from one valence band to another are forbidden by Pauli's exclusion principle. Our approach to this is very simple and effective. For a given $\mathbf{k}$, instead of solving the time evolution equation (11) just once for the eight electrons, we propose solving this equation four times, one for each valence band, neglecting the other three.

VII. SPLIT-OPERATOR METHOD

We obtained numerical solutions of the time-dependent Schrödinger equation (11) considering the split-operator method. It is well known that a general solution of

$$i\frac{\partial}{\partial t}|\phi(t)\rangle = H(t)|\phi(t)\rangle \tag{19}$$

is given by

$$|\phi(t)\rangle = \exp\left[-i\int_{t_0}^{t} H(\tau)d\tau\right]|\phi(t_0)\rangle \ . \tag{20}$$

This can be used to obtain an algorithm to calculate the wave function at a time $t+\delta t$, provided that the wave function is known at the time t.

Moreover, if the step δt is small enough, it is possible to consider that the Hamiltonian is nearly constant between t and $t+\delta t$. Then the evolution operator is considerably simplified,

$$|\phi(t+\delta t)\rangle = e^{-iH(t)\delta t}|\phi(t)\rangle \ . \tag{21}$$

This expression for the evolution operator is not suitable for an easy numerical computation. It is much better to split the evolution operator into two parts, one with the crystal Hamiltonian, and apply them consecutively, which can be done, of course, for small time steps δt. It is well known that the split-operator algorithm suitable to calculate the time evolution of the wave function is

$$|\phi(t+\delta t)\rangle = \exp[-iH_{\rm int}(t+\delta t)\delta t/2]e^{-iH_c\delta t} \times \exp[-iH_{\rm int}(t)\delta t/2]|\phi(t)\rangle \ . \tag{22}$$

The application of each of the exponential operators is preceded by the projection of the time-dependent wave function over the basis of eigenfunctions. The action of the operator on each element of this basis is reduced to a multiplicative phase. Therefore, using the plane-wave expansions of the Bloch functions (18) and the time-dependent wave function (16) one finally obtains the algorithm for calculating at each time step the β coefficients,

$$\beta_{\mathbf{k}+\mathbf{g}}(t+\delta t) = \exp\left[-i\left[\frac{1}{2c^2}A^2+\frac{1}{c}A(k_z+g_z)\right]\delta t\right] \times \sum_{\mathbf{g}'}\beta_{\mathbf{k}+\mathbf{g}'}(t)\gamma(\mathbf{g}',\mathbf{g}) \tag{23}$$

with

$$\gamma(\mathbf{g}',\mathbf{g}) = \sum_n \alpha_{\mathbf{g}'}^{\mathbf{k},n\,*} e^{-iE_n^{\mathbf{k}}\delta t}\alpha_{\mathbf{g}}^{\mathbf{k},n} \ . \tag{24}$$

The advantage of this method is that one directly obtains the β coefficients, from which it is straightforward to calculate the dipole moment, therefore the method is absolutely appropriate for the final variables we want to compute.

Observe that in (23) the coupling between two Bloch functions $\psi_{\mathbf{k},n}$ and $\psi_{\mathbf{k},n'}$ is accounted for in the $\gamma(\mathbf{g}',\mathbf{g})$ coefficients. The useful point is that these couplings are time independent, therefore one needs to calculate them just once at the beginning of the computation.

VIII. COMPUTED RESULTS

We show in the present paper numerical results for different values of the laser frequency, analyzing how they lead to different harmonic spectra. We have chosen the frequencies, that we consider more representative, from the joint density of states weighted by the squared transition matrix elements,

$$J_M(\omega) = \sum_{i,\rm VB}\sum_{j,\rm CB}\int_{\rm BZ}\delta(\omega_{ij}(\mathbf{k})-\omega)|M_{ij}(\mathbf{k})|^2 d^3k \ , \tag{25}$$

where $\omega_{ij}(\mathbf{k}) = E_j^{\mathbf{k}} - E_i^{\mathbf{k}}$ is the difference of energies between the bands i and j for this value of $\mathbf{k}$, $M_{ij}(\mathbf{k})$ is the transition matrix element, and the index i scans the four valence bands while the index j scans all the conduction bands considered.

This joint density of states is helpful in these kind of treatments because it is closely related to the imaginary part of the complex dielectric constant,[5] and gives an estimation of the one-photon transition probabilities. The joint density of states $J_M(\omega)$ calculated for pure silicon, with the considered pseudopotential, is shown in Fig. 2.

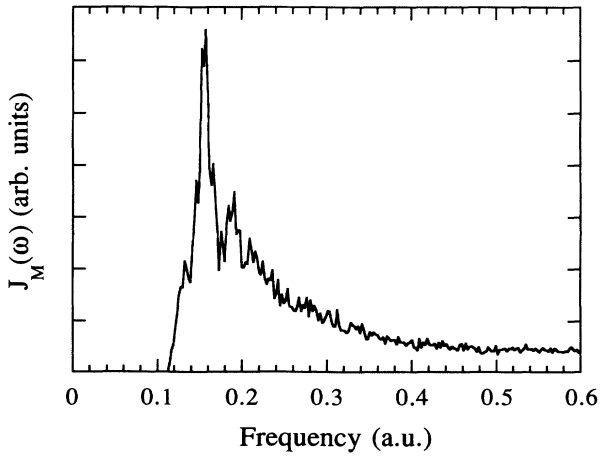

FIG. 2. Joint density of states weighted by the squared transition matrix elements, $J_M(\omega)$, calculated for pure silicon, with the considered pseudopotential.

It vanishes below $\omega_L = 0.11$ a.u., then increases abruptly and presents a sharp peak at $\omega_L = 0.16$ a.u. After the maximum, the joint density drops off very quickly, because the weighting matrix element rapidly decreases. It has a local minimum at $\omega_L = 0.18$ a.u., and then for higher frequencies the behavior is smooth and steadily decreasing, as is well known. We will use these two frequencies, $\omega_L = 0.16$ and 0.18 a.u., as reference points to understand the numerical results.

Observe that all calculations have to be integrated over **k**. This introduces some extra numerical complexity. What we have done instead, to introduce a set of points in the reciprocal space to account for the integration, has been to randomly generate values of **k** in the first octant ($k_x \geq 0; k_y \geq 0; k_z \geq 0$). To keep parity very accurate, we make the calculation for **k** and $-\mathbf{k}$. And finally, because of the symmetry around the field polarization axis, we multiply the result by 4. With these considerations we have observed that spectra are clearly defined with 125 random points in the first octant. Introducing more points in the numerical integration does not affect significantly the profile of the harmonic spectra.

Results for $\omega_L = 0.160$ *a.u.* This corresponds to a laser frequency resonant with the direct gap, and therefore is associated to the maximum in the joint states density shown in Fig. 2.

In this case the one-photon process from the top of the valence band to the bottom of the conduction band is resonant and is expected to be the dominant feature in the harmonic-generation spectra. This is clear in Fig. 3, which shows the spectra for three different intensities of the laser field. Figure 3(a) corresponds to $E_0 = 0.0003$ a.u., a rather low value, which is consequently absolutely dominated by the one-photon process giving just the fundamental frequency with the corresponding power broadening. Figure 3(b) corresponds to $E_0 = 0.001$ a.u., still a low value, which again just presents the fundamental frequency with the corresponding power broadening. Figure 3(c) corresponds to $E_0 = 0.003$ a.u., 100 times more intense than in the first case, showing now a small three-photon peak.

In this paper we want to study harmonic generation in a nondestructive way. We restrict ourselves to intensities such that just a small fraction of the electron population is promoted to the conduction band. To be more precise, we plot the population of the four valence bands and neglect intensities such that more than five % of the electrons are promoted to the valence band. Results for the highest field considered, $E_0 = 0.003$ a.u., are shown in Fig. 4. This figure indicates the time evolution of the electronic population of each of the four valence bands, integrated over the first Brillouin zone. The population in each band has been normalized to unity. It is clear that one of the bands, the lowermost—labeled as the first band in the figure—does not contribute to the electronic excitation, just because it is far below the band gap. The contribution of the second band is also very small. However, the contribution of the third band and the fourth band—the uppermost—is important. Both show a typical characteristic profile during the evolution of the pulse. They present a minimum at the peak of the pulse and they come closer to the initial state at the end of the pulse. This is due to our choice of a smooth pulse envelope (10), and is well understood in terms of adiabatic following in a two-level system.[14] The depletion of the fourth band is greater than the depletion of the third one

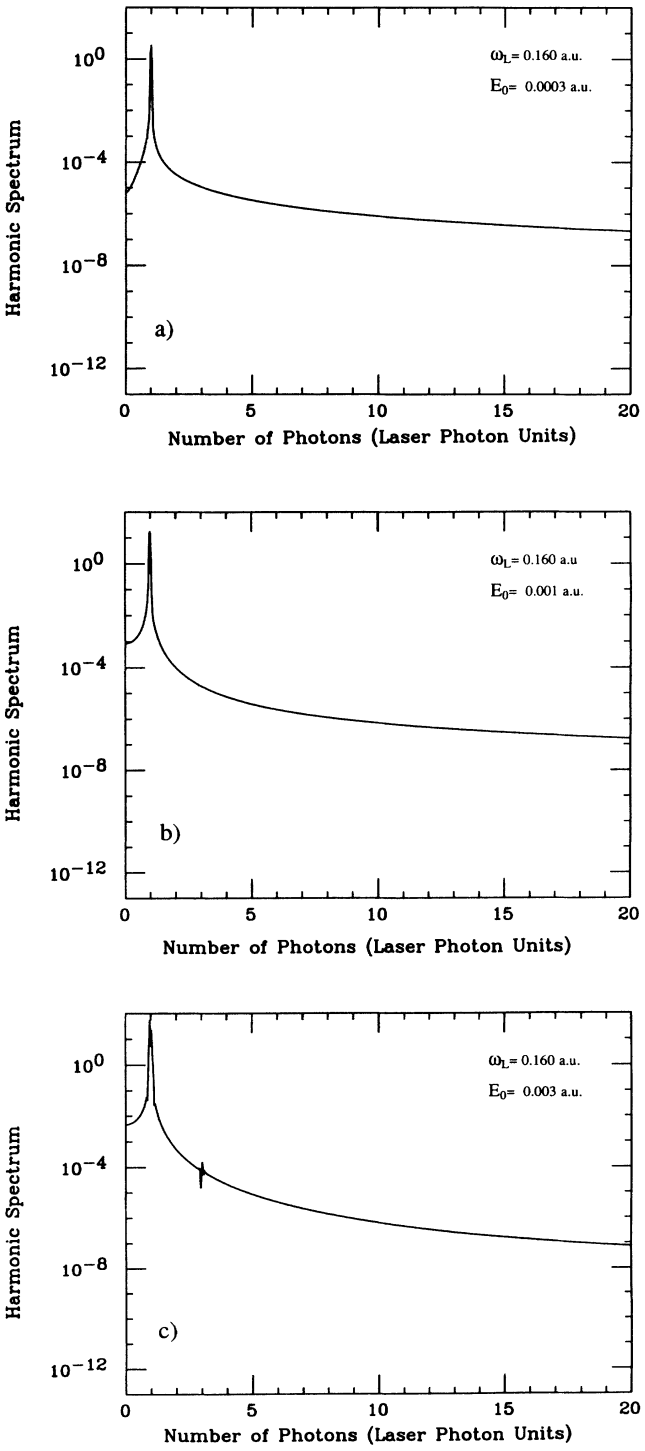

FIG. 3. Coherent harmonic-generation spectra, for an incident frequency $\omega_L = 0.160$ a.u. and three values of the peak electric-field amplitude, $E_0 = 0.003$, 0.001, and 0.003 a.u. Figure shows photon spectra $|p(\omega)|^2$ in a.u. vs harmonic frequency, scaled to the incident laser frequency ω_L.

because it is closer to resonance. The laser frequency chosen is very close to the difference between the highest valence band and the lowest conduction band. The depletion of the valence bands indicates a strong absorption of the laser field. Therefore a laser pulse of this frequency cannot penetrate the bulk material. To avoid this problem we will consider laser frequencies smaller than the energy gap.

Results for $\omega_L = 0.080$ *a.u.* This corresponds to a two-photon resonance with the direct gap. Figure 5 shows the harmonic generation in this case. Because this is a two-photon resonance, some signal tries to appear at twice the initial frequency, however this is forbidden by parity and therefore is very small and noisy. A three-photon peak [Fig. 5(a)], a five-photon peak [Fig. 5(b)], and a seven-photon peak [Fig. 5(c)] can be clearly seen.

Results for $\omega_L = 0.053$ *a.u.* This corresponds to a three-photon resonance with the direct gap. Figure 6 shows the harmonic generation in this case. Because this is a three-photon resonance, a stronger signal appears at three times the initial frequency. A three-photon peak [Fig. 6(a)] and a five-photon peak [Fig. 6(b)] can be clearly seen. The seven-photon peak [Fig. 6(c)] is very small. Because this is a three-photon resonance, the three-

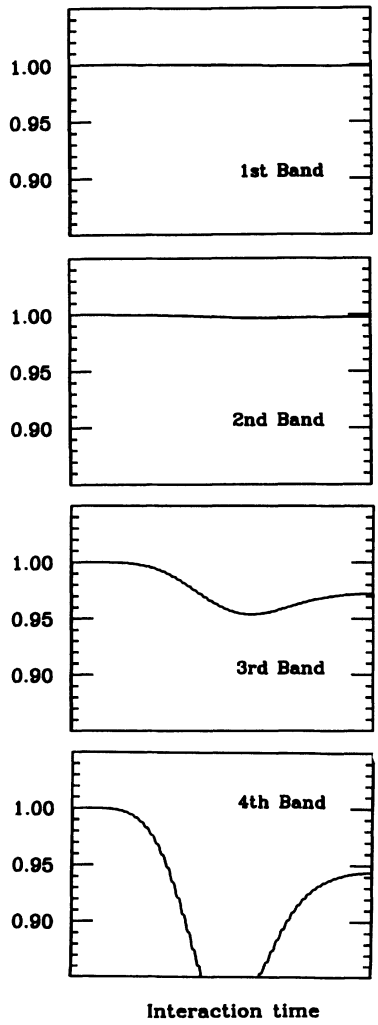

FIG. 4. Time evolution of the population of the four valence bands, for $\omega_L = 0.160$ a.u. and $E_0 = 0.003$ a.u. Bands are labeled according to their energy, for each **k**. The first band is the lowest and the fourth the highest. Time corresponds to the pulse duration, the pulse peak being just at the middle.

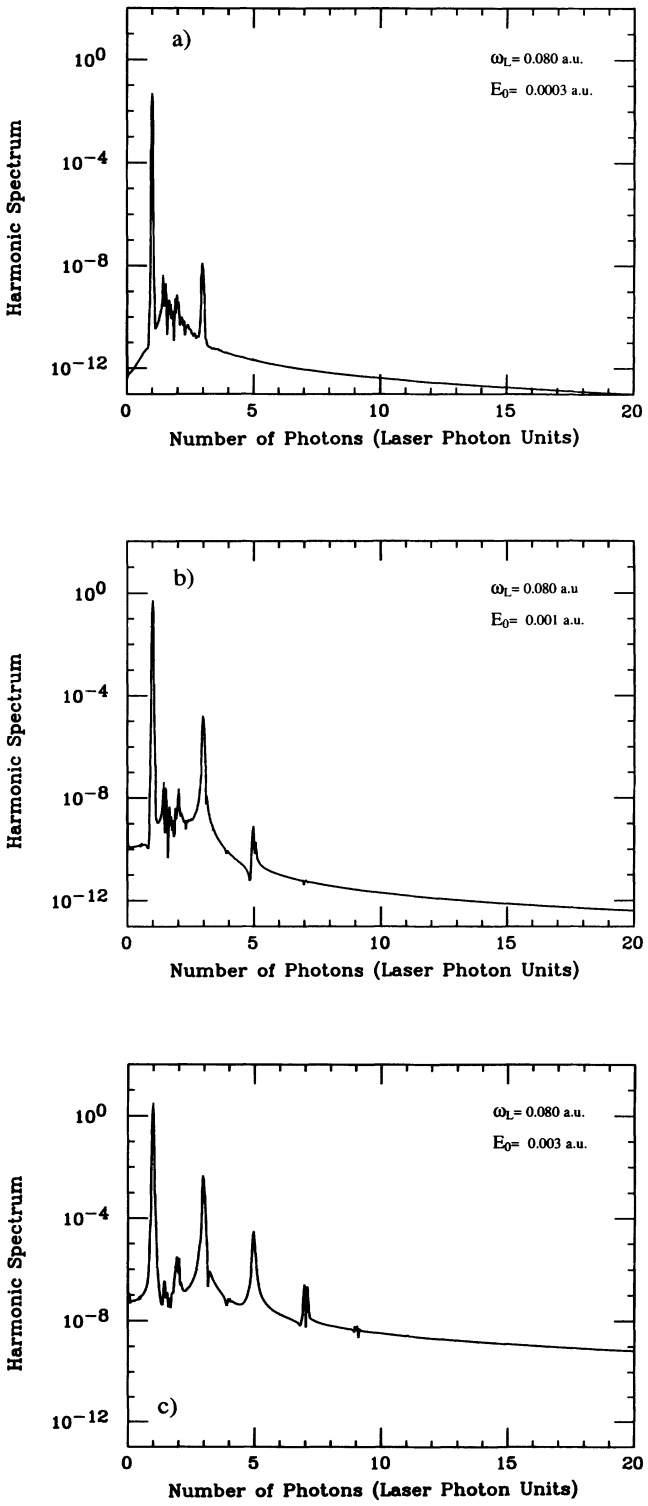

FIG. 5. Coherent harmonic-generation spectra, for an incident frequency $\omega_L = 0.080$ a.u. and three values of the peak electric-field amplitude, $E_0 = 0.0003$, 0.001, and 0.003 a.u.

photon peak shows a broadening that looks like the broadening of the one-photon peak in Fig. 3.

Results for $\omega_L = 0.180$ *a.u.* This corresponds to a laser frequency equal to the minimum in the joint density of states show in Fig. 2. Figure 7 shows the harmonic gen-

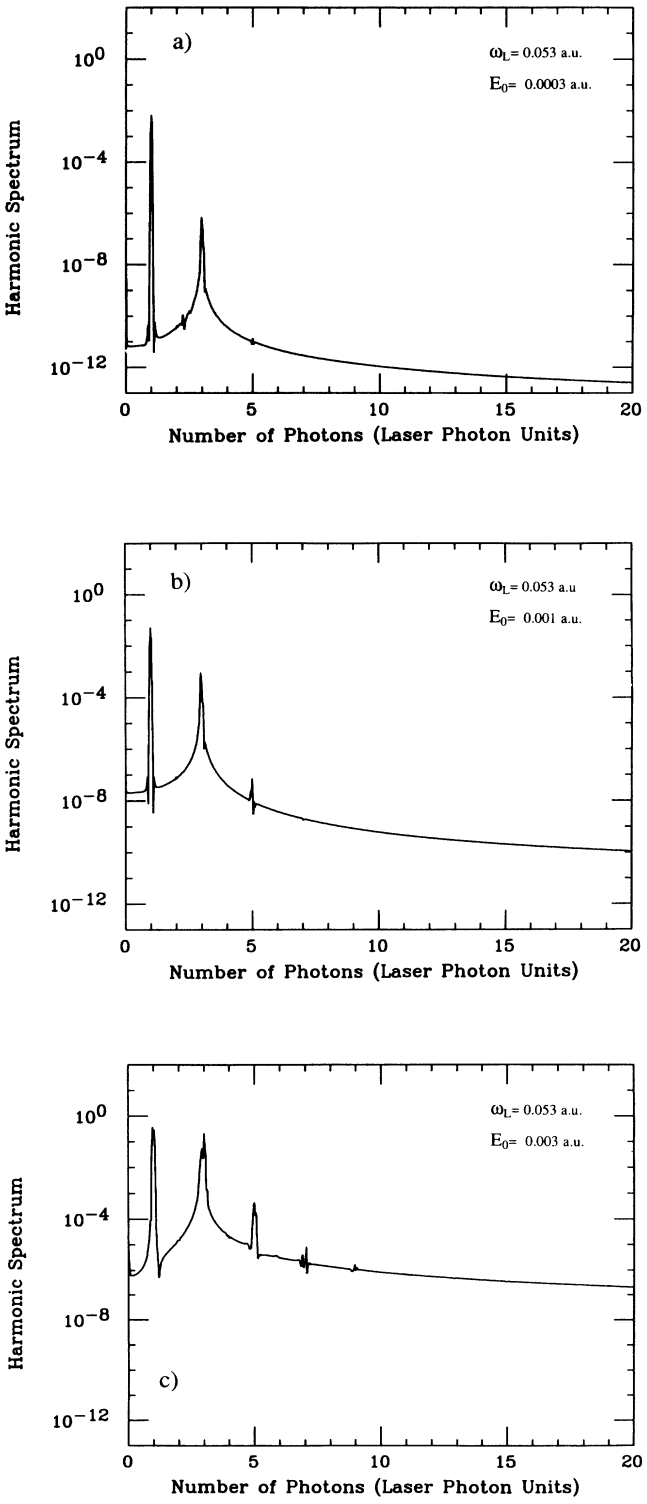

FIG. 6. Coherent harmonic-generation spectra, for an incident frequency $\omega_L = 0.053$ a.u. and three values of the peak electric-field amplitude, $E_0 = 0.0003$, 0.001, and 0.003 a.u.

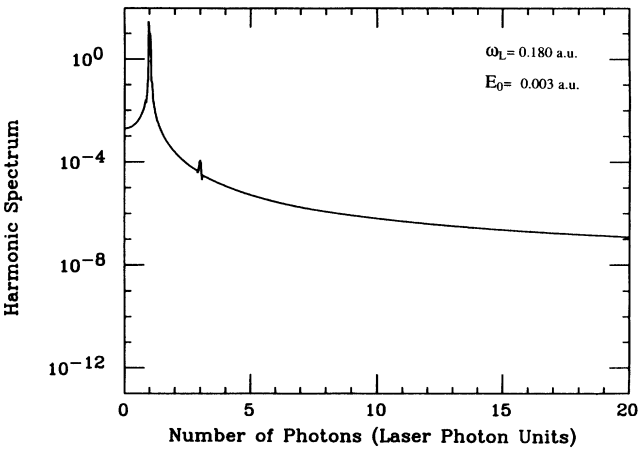

FIG. 7. Coherent harmonic-generation spectra, for an incident frequency $\omega_L = 0.180$ a.u. and a peak electric-field amplitude $E_0 = 0.003$ a.u.

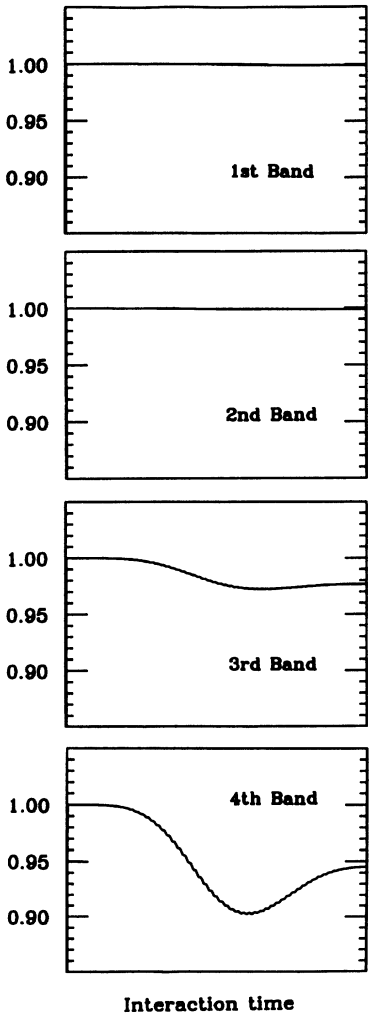

FIG. 8. Time evolution of the population of the four valence bands, for $\omega_L = 0.180$ a.u. and $E_0 = 0.003$ a.u. Bands are labeled according to their energy, for each **k**. The first band is the lowest and the fourth the highest. Time corresponds to the pulse duration, the pulse peak being just at the middle. Compared with Fig. 4, much less electronic population is excited for the same value of the electric field.

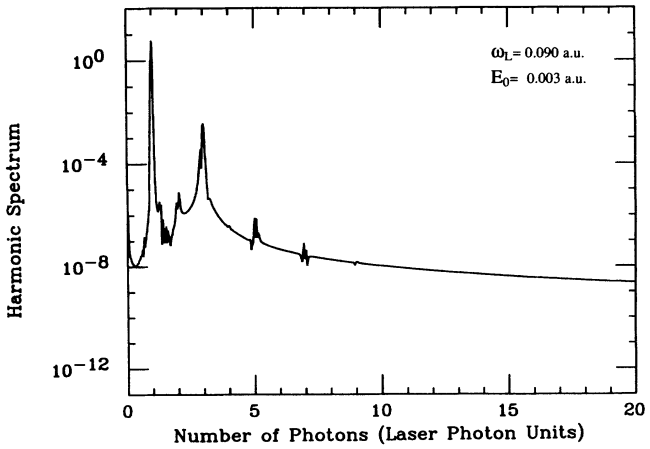

FIG. 9. Coherent harmonic-generation spectra, for an incident frequency $\omega_L = 0.090$ a.u. and a peak electric-field amplitude $E_0 = 0.003$ a.u.

eration in this case. Because this is again a one-photon resonance, the stronger signal appears just at the initial frequency. The harmonic spectra shown in Figs. 3 and 7 are very similar. The only difference is that the first corresponds to the maximum in the joint density and the last to the minimum. However, the important difference between these two cases is the time evolution of the electron population. Figure 8 shows the time evolution of the electronic population of each one of the four valence bands integrated over the first Brillouin zone. The population in each band has been normalized to unity. It is again clear that one of the bands, the lowermost, does not contribute to the electronic excitation, just because it is far below the band gap. Observe that the minimum of the population of the valence bands at the pulse peak is now much higher than that in the case of Fig. 4.

Results for $\omega_L = 0.090$ *a.u.* This corresponds to a two-photon process resonant with the minimum in the joint density of states shown in Fig. 2. The harmonic spectrum for $E_0 = 0.003$ a.u. is shown in Fig. 9. Again, it is similar to the spectrum in Fig. 5(c), with the only difference being that now much less population has been excited to the conduction band.

IX. CONCLUSIONS

A nonperturbative method to numerically compute solutions describing the interaction of an intense laser pulse with a crystalline structure has been presented. The crystal electrons are described in terms of a pseudopotential, and the laser field is described classically. The case of pure silicon has been specifically studied. Special attention has been paid to the possibility of nondestructive harmonic generation. We have studied laser frequencies below and above gap resonance. Harmonic generation proves to be more feasible in the first case, since resonant one-photon processes are weak. Also population pumping to the excited states is much weaker, therefore a pulse may reach deeper regions into the bulk.

ACKNOWLEDGMENTS

The authors want to thank K. Rzążewski for fruitful discussions. Support from the Spanish Dirección General de Investigación Científica y Technológica (PB 90 0725) and from NATO (CRG 900352) is acknowledged.

*Also at Departament de Matematica Aplicada, Escola d'Estudis Empresarials, Universitat Pompeu Fabra, 08002 Barcelona, Spain.

†Present address: Departament de Física, Universitat Autònoma de Barcelona, 08193 Bellaterra, Spain.

[1]J. H. Eberly, O. Su, J. Javanainen, K. C. Kulander, B. W. Shore, and L. Roso-Franco, J. Mod. Opt. **36**, 829 (1989).

[2]J. H. Eberly, J. Javanainen, and K. Rzążewski, Phys. Rep. **204**, 331 (1991).

[3]N. Sarukura, K. Hata, T. Adachi, R. Nodomi, M. Wanatabe, and S. Wanatabe, Phys. Rev. A **43**, 1669 (1991).

[4]L. A. Lompre, A. L'Huillier, M. Ferray, P. Monot, G. Mainfray, and C. Manus, J. Opt. Soc. Am. **7**, 754 (1990).

[5]M. L. Cohen and J. R. Chelikowsky, *Electronic Structure and Optical Properties of Semiconductors*, edited by M. Cardona, Springer Series in Solid State Sciences Vol. 75 (Springer, Berlin, 1989).

[6]V. Heine, M. L. Cohen, and D. Weaire, in *Solid State Physics*, edited by H. Ehreinreich, F. Seitz, and D. Turnbull (Academic, New York, 1970).

[7]F. Bassani and M. Yoshimine, Phys. Rev. **130**, 20 (1963).

[8]L. Kleinman and J. C. Phillips, Phys. Rev. **118**, 1153 (1960).

[9]M. L. Cohen and T. K. Bergstresser, Phys. Rev. **141**, 789 (1966).

[10]The IMSL Library. A set of FORTRAN subroutines for mathematics and statistics, 9th ed. IMSL Inc., 1982.

[11]W. H. Press, B. P. Flannery, S. A. Teukolsky, and V. T. Vetterling, *Numerical Recipes. The Art of Scientific Computing* (Cambridge University Press, Cambridge, 1988).

[12]R. M. Potvliege and R. Shakeshaft, Phys. Rev. A **40**, 3601 (1989).

[13]R. Tsu, R. T. Hodgson, T. Y. Tan, and J. E. Baglin, Phys. Rev. Lett. **42**, 1356 (1979).

[14]See, for example, L. Allen and J. H. Eberly, *Optical Resonance and Two-Level Atoms* (Dover, New York, 1987), Chap. 3, and references therein.